Infrared Physics & Technology 60 (2013) 145–154

Contents lists available at SciVerse ScienceDirect

Infrared Physics & Technology

journal homepage: www.elsevier.com/locate/infrared

Passive IR field gradient detection of thermal objects in active Fresnel zones

Faisal Rafique [a,*], Najeeb Siddiqui [b]

[a] Department of Applied Physics, University of Karachi, Pakistan
[b] Department of Electronic Engineering, Sir Syed University of Engineering & Technology, Pakistan

HIGHLIGHTS

- PIR scanner system that map IR radiation from static thermal sources through each Fresnel lens in an array.
- Our approach consisting four Fresnel zones and system is comparatively less costly.
- A fast Pattern matching achieved using DTW on STFT reduced length time vectors.
- Monitoring zones are easily configurable by increasing number Fresnel lenses.
- This system can be used to monitor hot points of power grid to surveillance system.

ARTICLE INFO

Article history:
Received 10 July 2012
Available online 29 April 2013

Keywords:
Thermal patterns
Thermal field gradient
Passive infrared (PIR)
Fresnel zones
Dynamic time warping (DTW)
Shot Time Fourier Transform (STFT)
Data acquisition (DAQ)

ABSTRACT

A dual element Passive-Infrared (PIR) sensor is used with a rotating slit aperture to map a narrow scanning beam on the sensing elements through each lens of a Fresnel lens array. The stimuli generated due to each thermal object fall in the active Fresnel zones in a certain direction based on their locations and temperature variations on the surfaces of the sources. These signals are used to analyze the signatures of stationary thermal objects, their slight movements and thermal field gradient changes of the source surfaces provided the object projected area is less than the area of the active zone. Pattern matching is performed using Dynamic-Time-Warping (DTW) algorithm on STFT reduced length time vectors. The object space is divided into m-active zones that correspond to the Fresnel zones in a Fresnel lens array. Within passive IR region from each of the active zones, the system identifies not only the heat intensity changes but also detects the slight movement of the thermal source. The efficiency of the system is dependent on the number of active Fresnel zones and the angular separation between them. This single node PIR sensor system is designed to cover an angular view of $\sim 10^\circ \times 80^\circ$ while horizontal Field of View (FOV) is divided into 4 active Fresnel zones. Generally costly Thermal-IR camera is used for thermal analysis. Our system is comparatively less costly and active coverage zones are easily configurable by increasing number of Fresnel lenses.

© 2013 Elsevier B.V. All rights reserved.

1. Introduction

1.1. Major area of PIR sensor application

In surveillance systems the capacitive charge displacement pyroelectric infrared sensor (PIR) is not only one of the crucial element but also provide a fast and cost effective solution of detecting warm body movements in the active inspection zones. In construction of a PIR system, Fresnel lens and mirrors are used to focus and shape the infrared radiation from certain inspection zones to the sensors die. In applications these sensors have been used in passive IR motion tracking systems utilizing coded apertures [1], burglar alarm system [2], door and camera actuators and entering/exit counter systems [3–5], as a part of a biometric system [19], flame detection [20], IR thermometry and pyrometers. PIR sensors based system was proposed for target tracking and angle-only measurements of the target from missile [13], in intelligent system to distinguish humans from other warm blooded animals, tracking and detecting path dependent and independent gait recognition and classification systems [8–11].

1.2. Sensor design and spectral parameters

Humans and other warm blooded animals skin radiate heat with wavelength between 8 μm to 14 μm in the thermal IR region. The skin temperature of a normal human being is 32 °C/89.6 °F/305.15 K. From Stefan–Boltzmann law, intensity temperature relation is;

* Corresponding author. Tel.: +92 219261300/2258.
E-mail address: faisal.rafique@uok.edu.pk (F. Rafique).

1350-4495/$ - see front matter © 2013 Elsevier B.V. All rights reserved.
http://dx.doi.org/10.1016/j.infrared.2013.04.007

$$I = \varepsilon_m \sigma T^4 \quad \text{where } \sigma \text{ (Stefan–Boltzmannconstant)} = 5.67 \times 10^{-8}\ \mathrm{W/m^2\ K^4} \tag{1}$$

With the emissivity ε_m of 0.98 for the human skin and without masking by cloths, the total radiated intensity I at 305.15 K is 481.79 W/m^2.

The frequency Temperature relation is given by the Wein's law

$$F_M = wT_A \quad \text{where } w \text{ (Wein's constant)} = 1.035 \times 10^{11}\ \mathrm{Hz/K} \tag{2}$$

For humans the radiated frequency F_M for maximum radiated intensity obtained at 310.15 K skin temperature is 32.1 THz and the corresponding wavelength is 9.5 μm, which falls in the thermal infrared region of EM spectrum. For most of the commonly available PIR sensors with adequate beam focusing it is possible to detect human movement at a distance of several meters from sensor present inside and in the vicinity of the active Fresnel zones. Besides humans, several other things with good emissive value emits EM radiation in thermal IR region which can be detected by a PIR sensor, e.g. a surface at 150 °C emit a lot of radiations with maximum intensity at 6.85 μm that comparatively at higher value than the level at lower temperatures, the large area under the Planck's curve can be detected at larger distances if it falls in the sensor's spectral window.

To detect the presence of an object based on its IR radiating heat energy waves, ferroelectric substances are used in manufacturing low cost passive infrared sensor. Materials such as Lithium Tantalate ($LiTaO_3$), Deuterated Triglycine Sulfate (DTGS), Lithium Niobate, Barium Titanate ($BaTiO_3$), Lead Titanate ($PbTiO_3$), and Polyvinylidene Fluoride (PVDF) exhibit dielectric current generation when exposed to heat radiation. The impedance across these capacitive charge displacement substances is around hundreds of giga-ohm, therefore their corresponding response time is too low in the range of mHz to few tens of Hz, thus suitable for detecting low speed moving thermal targets. Among these substances DTGS offers best pyroelectric voltage coefficient of $1.3 \times 10^6\ \mathrm{m^{-1}\ K^{-1}}$ and coupling coefficient of 7.5%, but DTGS is an expensive crystal, on the other hand sensors made from PVDF film or Lithium Tantalate as an active ingredient provide relatively low cost solution.

1.3. Thermal IR sensing element

In the experimental setup a dual element (series connected in opposite polarity) PIR sensor has been used. The PIR sensors are generally available in series/parallel connected dual and quadruple elements [6,16], multi-element PIR sensors are also manufactured in different electrical and geometrical designs. Generally a dual element PIR sensor is used in motion detecting systems based on temperature difference in contrast with the background or other adjacent objects including plasma and hot gases in an active zone, but in the proposed system the field modulation enable the sensor to monitor thermal field gradient of moving or even of static objects. As in a piezoelectric transducer, surface charge displacement dQ establishes when pressure waves are applied at piezo-sensitive material, therefore generating a proportional minute charge current. In the similar way when a pyroelectric material exposed to thermal IR radiation, a proportional electron drift is generated and then converted to voltage by a field effect transistor built into the case of the transducer connected in source follower configuration [7]. Dual element PIR sensor consists two chips of pyroelectric material connected serially in opposite polarity. When both elements exposed to same heat flux, an equal and opposite charge drift generated by both the elements and therefore the net drift becomes zero, this is the case when there is no temperature gradient inside the FOV of a Fresnel zone, the response shown by blue line (equal heat flux) in Fig. 1. But in a different case when heat flux covered by the partial red seek zone is greater than the other, a relatively large positive exponential voltage rising and falling appears at output terminal of the sensor due to the forward and reverse minute current i through elements, as depicted by red line in Fig. 1. As the distance from the sensor increases, the effective cross sectional area decreases, this effectively results in larger background thermal reference field, in this case the excitation from the elements becomes lowered.

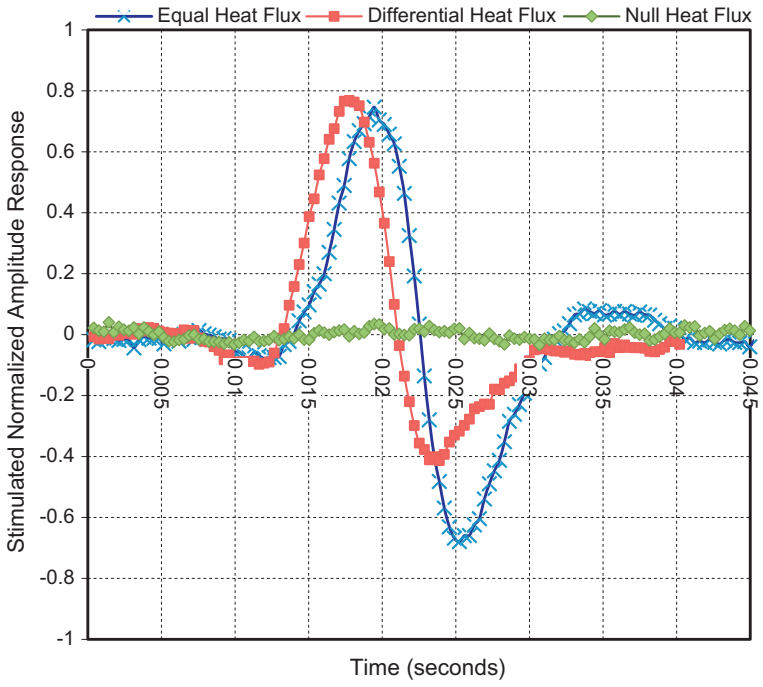

Fig. 1. Sensor responses: First response shown by blue line is the case when equal amount of heat flux from a static thermal source fall onto the sensor's elements. In second response shown by red line, a Fresnel zone partially exposed to heat flux. In third response, shown by green line, no significant thermal source present in the active zone.

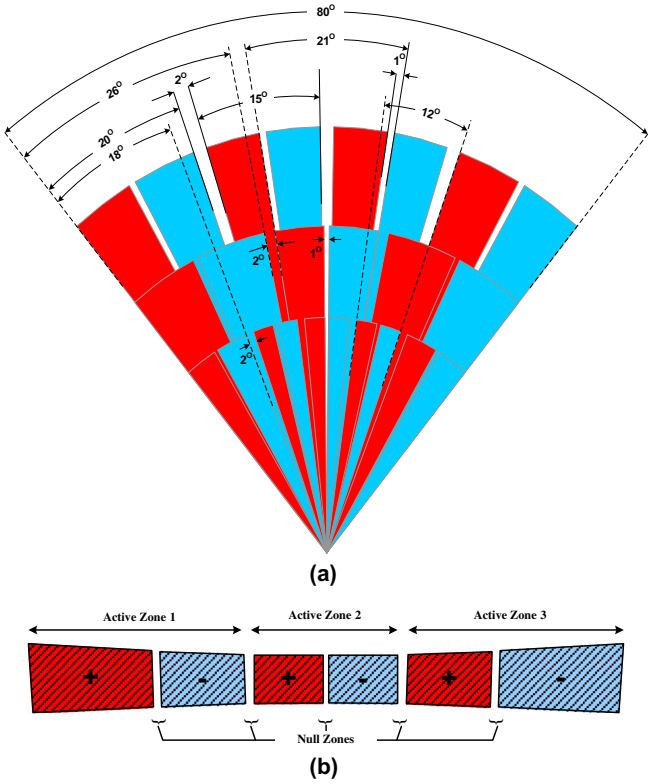

Fig. 2. (a) Fresnel zones/seek zones of three different lens arrays are shown. For 3-lens Fresnel zones: side zones (1st, 3rd) are 26° and mid zone (2nd) of 21°. For 5-lens Fresnel zones: 1st, 5th are 18°; 2nd, 4th are 12° and 3rd is 7°. For 4-lens Fresnel zones: 1st, 4th are 20°; 2nd, 3rd are 15°. All arrays have 2° zone and 1°subzones separation. (b) Planer view of projected 3 lens array onto the object space indicating active Fresnel zones & null zones.

1.4. Pyro-sensor modeling

The IR radiant flux Φ_e forms a focused thermal image on the sensor's element by the Fresnel lens. This flux generates a temperature drift dT in the element that produces a change in polarization P resulting in an electrical charge displacement dQ. Thus the rate $\Delta P/\Delta T$ or the rate of the equivalent charge displacement with the temperature change on the surface of the pyro element is directly proportional to the surface area s with the electron drift per unit area and temperature change; this is called Pyro-Coefficient denoted by p. When a pyrosensitive element having thickness d, surface area s and specific heat c, exposed to thermal flux Φ_e, an increasing temperature drift with time causes increase in incident flux. The minute current generated is thus defined as [15]:

$$i = \left(\frac{p}{cd}\right)\Phi_e \tag{3}$$

The minute current i generated by a pyrosensitive element due to the temperature difference between source at T_2 (K) and the element at T_1 (K) with related emissivity, transmissivities and other related parameters can be determined by Stefan–Boltzmann's law:

$$i = \frac{ps^*\gamma_c\gamma_w\varsigma_{fl}}{2\pi cd}\varepsilon_s\sigma\left(\frac{T_2^4 - T_1^4}{r^2}\right) \tag{4}$$

$$where \quad \gamma_w = \begin{cases} 1 & |VFOV| > \frac{\pi}{4} \\ 0 & |VFOV| < \frac{\pi}{4} \end{cases} \gamma_c = \begin{cases} s\kappa & 0 < |HFOV| < \theta - \frac{\alpha}{4} \\ -s\kappa & \theta - \frac{\alpha}{4} < |HFOV| < \frac{\pi}{4} \\ 0 & -else- \end{cases} \tag{5}$$

where σ is the Stefan Boltzmann's constant, $s*$ is the total surface area of the thermal object, r is the distance of the lens from the source, ζ_{fl} is the transmissivity of the given Fresnel lens, γ_w is the attenuated field transmissivity in vertical field of view due to window; and γ_c is the transmisivity defined by chopped field due to modulating slit seeing the κ portion through the lens area s. Angle θ is the horizontal FOV of a single lens and angle α is the null zone angle i.e. angular separation between red and blue Fresnel zones.

1.5. Fresnel lens array

Thermal IR radiation can be easily blocked by ordinary glasses and plastics. Silicon or Germanium wafer is used as a filter to block the unwanted radiation from the source other than concerned IR band. To focus and shape the IR beam onto the sensor die, polyvinyle plastic Fresnel lens and mirrors are used. A Fresnel lens array generally consists several small lenses that corresponds to Fresnel zones, active zones or seek zones.

Fresnel lenses are generally made from acrylic, rigid vinyl and polycarbonate plastics, each having different transmittance properties. In this research we used Fresnel lens made of POLY-IR 2 [12] material, each lens array contains 3, 4, and 5 stack of lenses, this material is transparent for wavelengths from 8 to 14 μm. Fig. 2 detailed the angular measurements of Fresnel zones and null zones. An active zone or Fresnel zone is a sectored volume where sensor is susceptible to react for thermal radiation. In null zones for any number of elements, sensor cannot register any temperature changing in the sector. Angular separation between adjacent differential field of views (FOV) within an active zone and between active zones for a dual element PIR sensor and Fresnel lens of 3, 4, and 5 stacks of lenses are shown in Fig. 2, in Fig. 2b the projection of the lens in Fig. 2a on object space is also shown. The red (dark) and blue (bright) FOV corresponds to the sensor's element.

2. Experimental setup and measurements

Fig. 3 shows the experimental setup which comprises of a scanning system, data acquisition, training and testing phases, pattern identification based on the lowest DTW scores of STFT reduced vectors and zone indicators that represent change in temperature

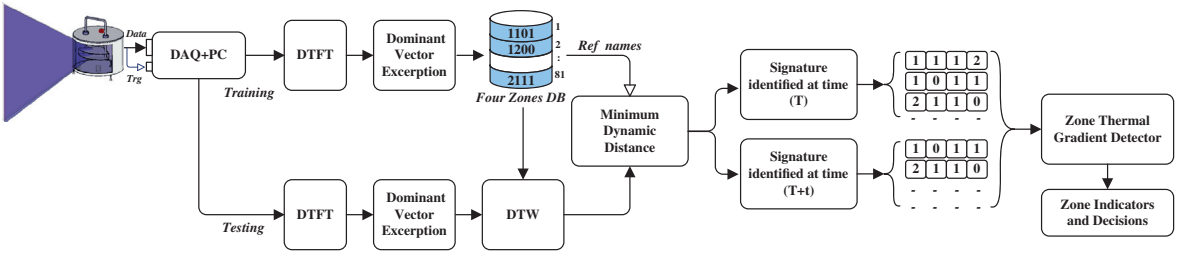

Fig. 3. Block diagram of thermal field gradient detection in monitoring zones based on three level temperature scheme indicated by 0, 1 and 2 that corresponds objects in the zones at 30 °C, 425 °C and 300 °C temperature respectively.

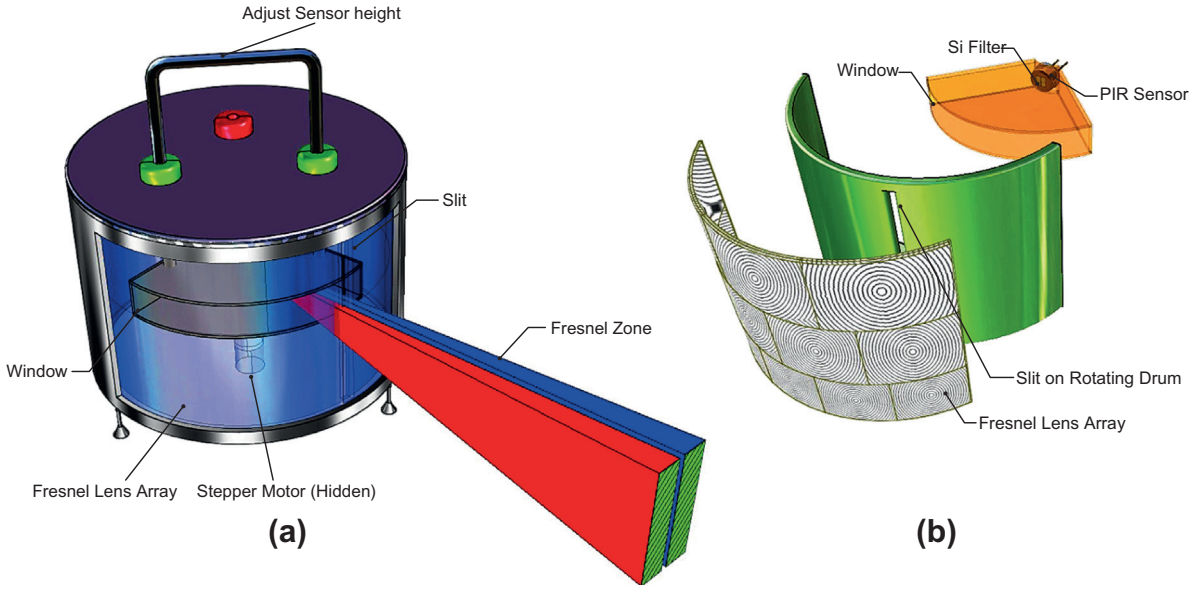

Fig. 4. PIR Scanner System (a) Complete assembly and (b) three parts form system spaces. (i) Object scanned space; (ii) rotating Aperture & window space or mapping space and (iii) measurement space including PIR sensor. All spaces modulate the thermal images from each zone.

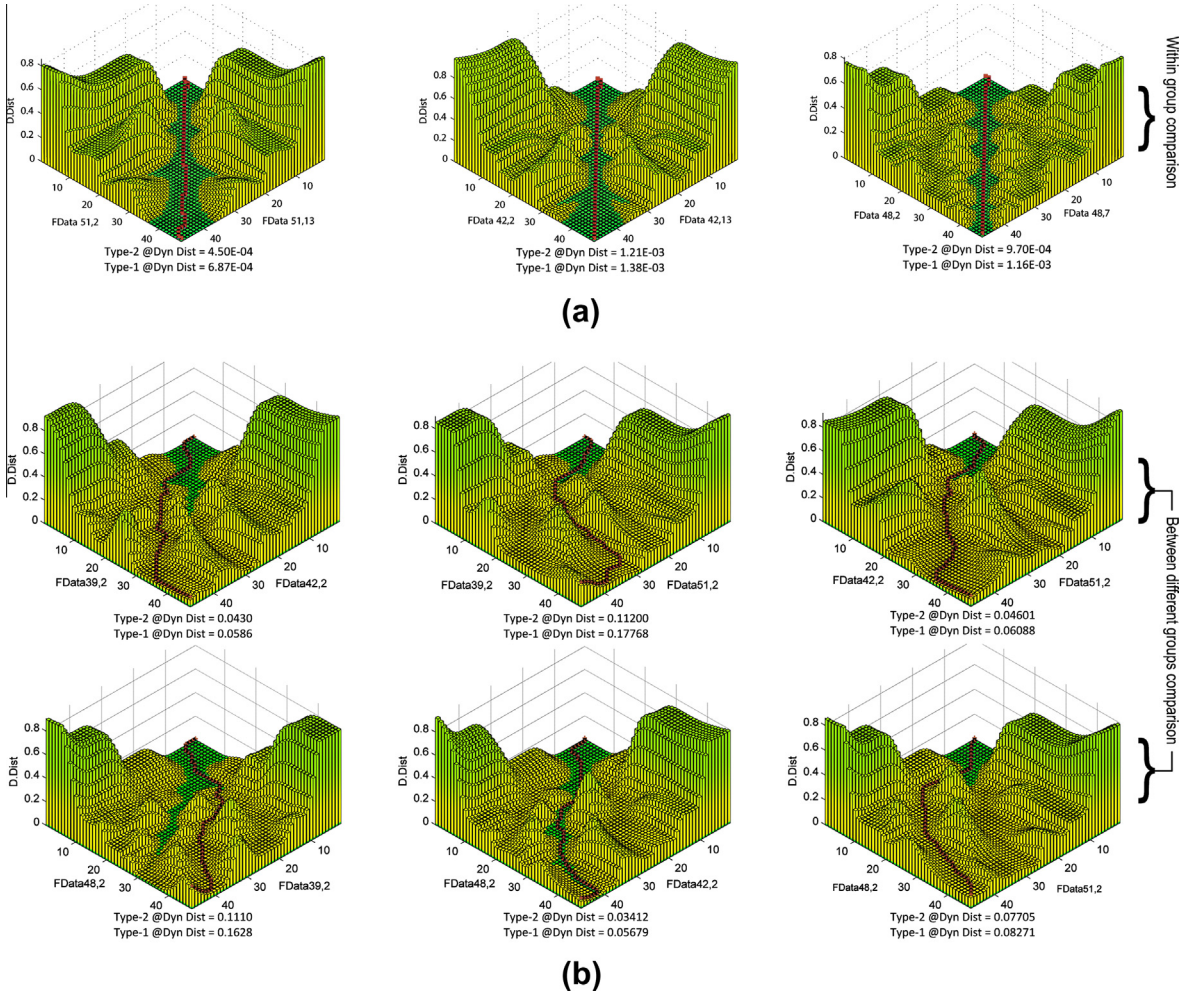

Fig. 5. Closest Warp path in the valley with type-2 galley path between the extracted STFT dominant time vectors of the four signatures [1 1 1 0] FData39, [1 2 1 0] FData48, [1 2 2 0] FData51 and [1 1 2 0] FData42. (a) Comparison within the same pattern group. (b) Comparison between groups. Vertical axis D.Dist is the local distance axis between *i*th and *j*th elements of the two series.

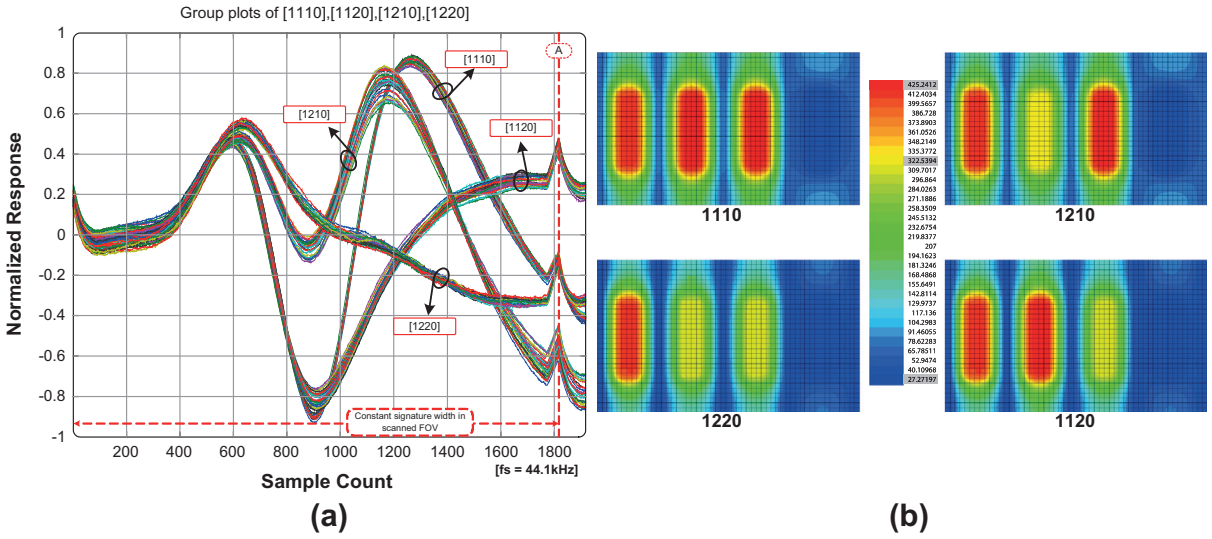

Fig. 6. (a) Four different signatures of 24 instances from a pool of 80 patterns, depicted large dissimilarities after sample count of 600. Four Fresnel zones monitored in this scan with zone-1 and zone-4 having thermal objects at 425°C indicated by '1' and 30 °C indicated by '0' respectively, while 300 °C indicated by '2'. Note that for signatures [1 1 1 0] and [1 1 2 0] the stimuli and polarity changes are almost the same up to sample count of ~900. (b) Simulated view of thermal contour patterns of the four signatures indicated (the separation between adjacent thermal objects are truncated in this figure).

in a zone. The scanning system of the experimental setup shown in Fig. 4 is designed to scan different active Fresnel zones for stationary objects emitting thermal radiations and generate combined thermal gradient response of these distributed thermal sources. This system contains four transmissive layers, as shown in Fig. 4b, in which fourth layer is a Si filter window of the sensor transparent to the concerned wavelength through which a part of thermal energy at an instant is projected to the sensor's die.

Each thermal object's surface area is $15'' \times 5''$ and separated from each other by $40''$. In this experiment these thermal objects placed at a distance of 10 feet inside each Fresnel zone. For shorter distances the dimension of the thermal objects should be reduced to avoid sensor's saturation. These objects emulate a reasonable size of, for example, electrical grids, power distribution boxes and actuators (motors, contactors, etc.) in power plants or industries. These power elements act as heat dissipating sources due to resistive contacts between wires, switch contacts, or actuators and can produce differential heat when a power element undergoes a sudden increase in power demand. In coded aperture schemes [1,8,9,19] the system only detect the movement of thermal sources and not sensitive to detect stationary thermal objects or their surface thermal variations, while our proposed thermal scanning system can detect thermal variations or surface thermal gradient of non moveable objects radiating thermal IR in specific Fresnel zones. We used three thermal gradient levels by having three different temperature levels. In this dual-element PIR sensor system, the rotating slit linearly scans through an active Fresnel zone to map thermal radiation to the first element and then to the second element. This mapped thermal radiation in a scan of an active Fresnel zone generates electrical signal which is further processed by the electrical circuit embedded in the sensor and then processed by the DTW algorithm.

A Fresnel lens assembly consisting of three linear arrays of multiple lenses is used. In the experiment an array of four lenses selected to monitor distinct radiant sources located in the four projected Fresnel zones; a Fresnel zone is shown by the two colored beam in Fig. 4a. Whole system is designed to reduce vibrations from rotating parts, because all pyroelectric materials are also piezosensitive. DAQ card installed in a PC collect and convert each sample of data into a 16 bit digital form at 44 kHz sampling rate. A batch process is developed to perform number of routines including STFT, DTW, database generator routine, and lens edge detector routine that pick the signals from an optocoupler and find the specific edges based on signal energy and power to trigger the data acquisition. In batch processing these edges reduces the code size; these edges are shown by instance 'A' in Fig. 6a.

A high input impedance high gain multistage operational amplifier installed inside the scanner system that can boost a sig-

Table 1
Comparison of Runtime and Scores of full length and STFT reduced length vectors using type-1 and type-2 DTW.

Pattern1	Pattern2	Full length Type-1		STFT Reduced Type-1		Full length Type-2		STFT Reduced Type-2		CSGOG type-1 (%)	CSGOG type-2 (%)	FSGOG (%)
		Score	Runtime (s)	Score	Runtime (s)	Score	Runtime (s)	Score	Runtime (s)			
1110/{39,2}	1220/{51,2}	0.0656	45.43	0.1777	0.11	0.048	46.69	0.112	0.12	0.387	0.402	3.89
1110/{39,2}	1120/{42,2}	0.0382	45.65	0.0586	0.11	0.0253	46.97	0.043	0.12	2.389	2.813	17.79
1120/{42,2}	1220/{51,2}	0.0463	45.68	0.0609	0.11	0.0347	47.08	0.046	0.11	1.13	0.978	−13.32
1210/{48,2}	1110/{39,2}	0.0962	45.46	0.1629	0.11	0.0775	45.95	0.111	0.11	0.736	0.873	18.63
1120/{42,2}	1210/{48,2}	0.0744	45.45	0.0568	0.12	0.0479	46	0.034	0.11	2.112	2.852	35.04
1220/{51,2}	1210/{48,2}	0.0728	45.31	0.0827	0.12	0.0534	46.83	0.077	0.11	1.451	1.259	−13.18
1120/{42,2}	1120/{42,13}	2.31E-04	45.32	0.0014	0.11	1.42E-04	45.99	0.00121	0.12			
1210/{48,2}	1210/{48,7}	9.74E-05	45.39	0.0012	0.13	6.37E-05	46.58	0.00097	0.11			
1220/{51,2}	1220/{51,13}	4.25E-04	45.46	6.87E-04	0.12	2.60E-04	46.11	4.50E-04	0.11			

FSGOG = Farness of Same Group to Outside the Group,% increase from type-1 to type-2.
CSGOG = Change from Same Group to Outside the Group.

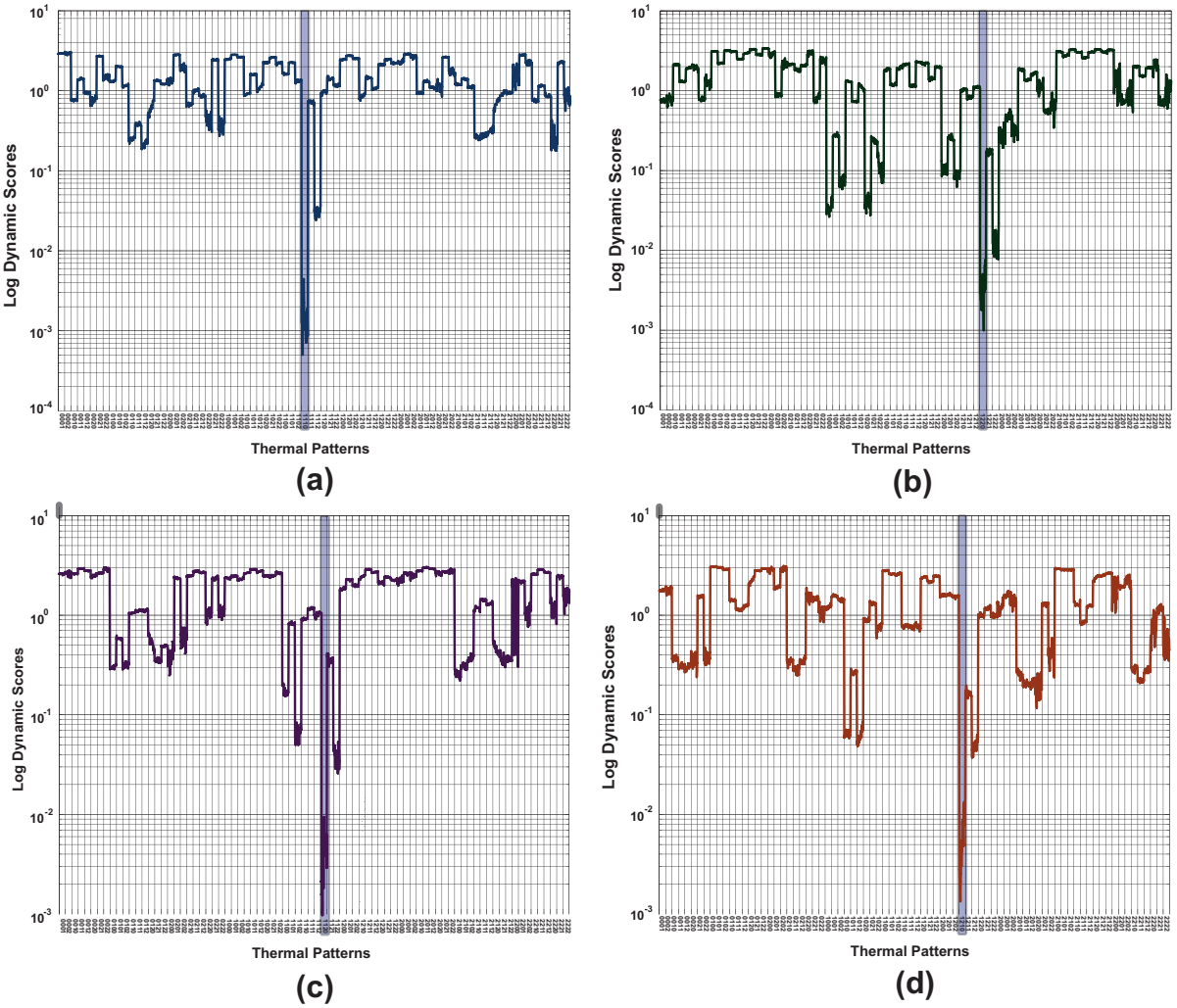

Fig. 7. Type-2 DTW Log dynamic scores of (a) [1 1 1 0] (b) [1 2 2 0] (c) [1 1 2 0] and (d) [1 2 1 0]. Plots depict minimum DTW scores produced when warped compared with their respective groups.

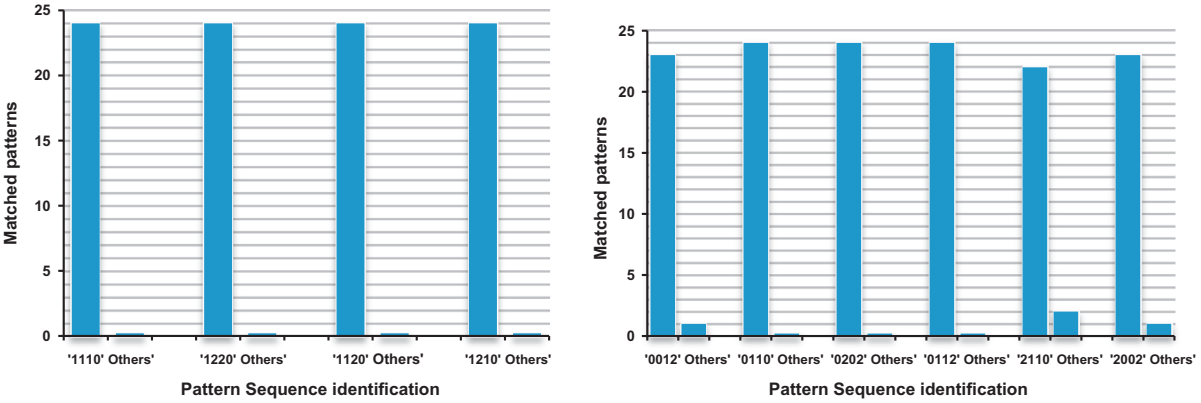

Fig. 8. Zone thermal gradient identification results of two random thermal pattern sequences for four Fresnel zones. Each database has first 24 STFT reduced vectors.

nal to a level to be detected by DAQ card from ten feet focused thermal source. Second layer of the system is a rotating slit; sensor sees through this slit, if the surface temperature of the source in the active zone remains the same for consecutive scans the signal portions for that scanned zone from dual elements remains the same, but any minor movement of the source at an angle with the direction of rotation or opposite generate a different signature. In an active zone a thermal field gradient can be detected when thermal flux in subzone changes. The size of the slit and the Fresnel lens is adjusted so that when the slit is in a sub Fresnel zone (+ve or

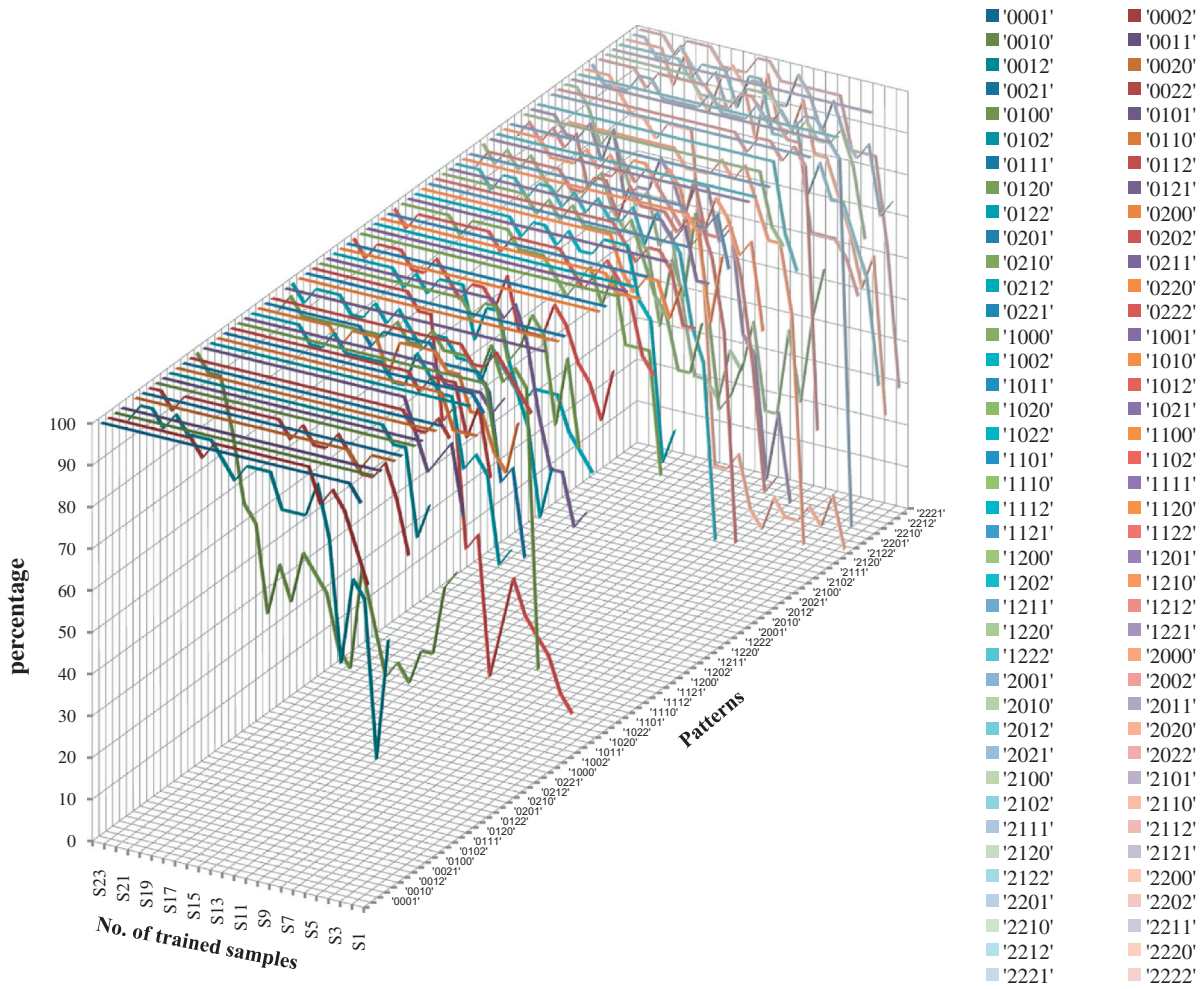

Fig. 9. Identification rates affected by the number of data samples of each pattern in the database. An optimum number of 24 samples found sufficient to produce recognition rates mostly higher than 95%.

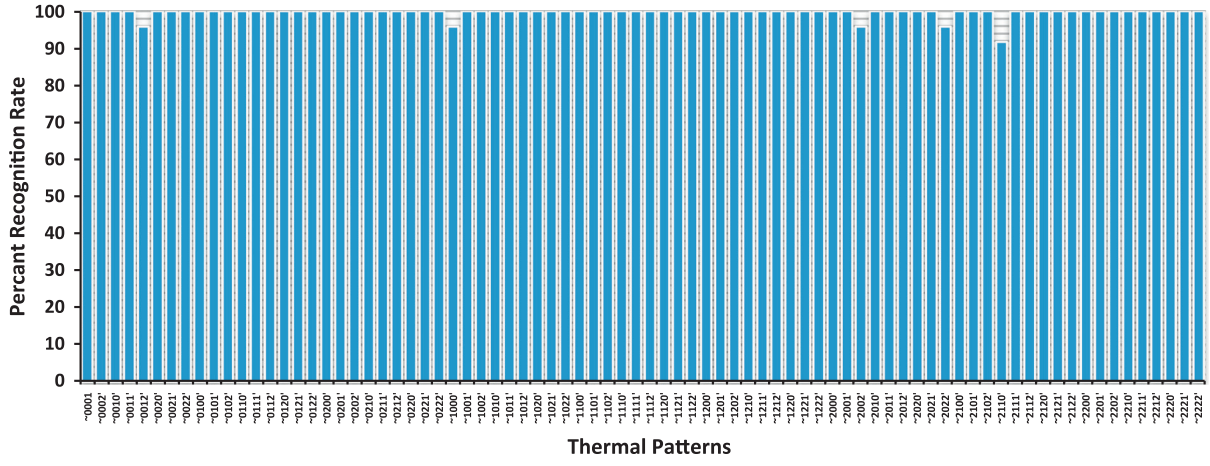

Fig. 10. Average identification rates of each registered thermal pattern for four Fresnel zones in 100 random sequences having all 80 thermal patterns. Database has 24 samples of each thermal pattern.

−ve), it maps thermal field to a single element only. To accelerate the signal polarity changing, a dual element PIR sensor was used in the experiment. As compared with a single element, a dual element PIR sensor produces electrical signals that can be easily separated by the analysis of their temporal and spectral responses.

In training and testing phases, STFT was used to extract dominant time vectors while in testing phase the STFT abstracted time vectors compared on the basis of global dynamic distances at different time instances. By comparing the detected pattern with the old stacked thermal patterns in the memory, the system can

Table 2
Test patterns that false matched with reference patterns. All other patterns have 0% false recognition rate with 2nd minimum dynamic distance.

Test patterns	False matched reference				
	2010′	1002′	0002′	0022′	0110′
0012′	4%				
1000′		4%			
2002′			4%		
2022′				4%	
2110′					8%

identify the behavior of thermal gradient field changes and recognize the current pattern based on the minimum dynamic score.

3. Methods

3.1. Short Time Fourier Transform

Fourier transform of a signal obtained in small time windowed section reveals time related event frequency information which cannot be observed by analyzing whole signal at a time; this is called Dennis Gabor adaptation or Short Time Fourier Transform and produces a two dimensional function $\boldsymbol{S_x(f,\ t)}$ of time and frequency, while in matrix notation columns represents frequency vectors and rows represents time vectors. STFT is applied on the discrete temporal signal $\boldsymbol{x(t)}$ to produce time-frequency information using overlapped sliding time window from which first close resemblance of reduced row vector is extracted that has largest influence over the entire length of the signal. For a discrete temporal signal $\boldsymbol{x(t)}$, the STFT is defined as:

$$S_x(f,t)=\begin{array}{c} \overset{f\ \text{vectors}}{\downarrow} \\ t\ \text{vectors}\rightarrow \end{array}\begin{bmatrix} \alpha_{11}^{i=0} & \alpha_{12}^{\circ} & \alpha_{13}^{\circ} & \cdots & \alpha_{1m}^{\circ} \\ [\alpha+i\beta]_{11}^{1} & [\alpha+i\beta]_{12}^{1} & [\alpha+i\beta]_{13}^{1} & \cdots & [\alpha+i\beta]_{1m}^{1} \\ \vdots & \vdots & \vdots & \ddots & \vdots \\ \vdots & \vdots & \vdots & \ddots & \vdots \\ [\alpha+i\beta]_{11}^{n-1} & [\alpha+i\beta]_{12}^{n-1} & [\alpha+i\beta]_{13}^{n-1} & \cdots & [\alpha+i\beta]_{1m}^{n-1} \end{bmatrix}=\sum_{k=0}^{m-1}x(\tau)\omega(t-\tau)e^{-j2\pi k} \tag{6}$$

The magnitude squared spectrum of Kaiser window STFT $|S_x(f,t)|^2_{K(n,\beta)}$ is used to find coefficients and total energy over entire period at certain frequency in the spectrum. STFT computed between onset and offset stimulus from optocoupler for each signal of sample size 1800 with Kaiser-window side lobe attenuation factor of 54dB. For high time–frequency resolution a fixed 97% overlapped window was used.

3.2. Dynamic time warping

Dynamic time warping is a pattern matching algorithm which was introduced by Sakoe and Chiba in 1978 [16], it is generally used in data mining, clustering and time series applications by finding similarity between data sequences. Modern speech recognition microcontrollers such as RSC-464 implemented DTW for speaker dependent identification [17]. DTW can be use to find instances at which a short time series appear with close similarity in a segment of a long sequence, thus one may think that DTW is an extension of the general character or word finding algorithms such as *Levenshtein distance*[18] applied on text data that yield 0 or 1 logics corresponding to a match. Using several constraints, DTW can be used in identification, classification and generate template database of data sequences based on minimum dynamic distances between them, using dynamic programming one can find best warping path even when the sequences shrinks or stretches in segments or in whole.A distinctive Data abstraction technique is used to speed up the recognition process. In this study type-2 DTW with five index search paths is applied on the reduced dimensionality time vectors extracted from STFT resolved time-frequency matrices. The first few resolved STFT vectors of short lengths are used to find dynamic distances that classify the signals with higher recognition rates and produces robust results. Suppose $X\{\alpha_{A1}, \alpha_{A2}, \ldots \alpha_{Ai}\} \in \mathbb{R}$ is a template vector and $Y\{\alpha_{B1}, \alpha_{B2}, \ldots \alpha_{Bi}\} \in \mathbb{R}$ is a test signal vector, the Euclidean local distance between each point of the sequences are calculated and multiple global distances within the warped window and with the constraint galley path estimated by summing indexed local distances from which the shortest global distance chosen, as shown in Fig. 5 for the selected patterns. The warping function $\boldsymbol{P}$ starts at the first index $i = j = 1$ of the two sequences and it is the sum of all possible local warp distances p in a neighborhood of a point that generally constrained by warping window or galley width and slope. The warping function $\boldsymbol{P}$ and window width $\boldsymbol{r}$ define as:

$$\boldsymbol{P}=\left\{p_{ij}\middle|i=1,2,\ldots,n\ j=1,2,\ldots,m\begin{matrix}\text{locus start at } p_{11}\\ \text{locus end at } p_{nm}\end{matrix}\right\} \tag{7}$$

$$r=|\alpha_{Ak}-\alpha_{Bk}|\ >\ 0\quad k=1,2,\ldots m\ \forall m\ \leqslant\ n \tag{8}$$

The cumulative distance up to the ith element of $\boldsymbol{\alpha_A}$ and jth element of $\boldsymbol{\alpha_B}$ is:

$$\delta(i,j)=d(\alpha_{Ai},\alpha_{Bj})+min\overbrace{\begin{cases}\delta(i-1,j).w_a\\ \delta(i-1,j-1).w_b\\ \delta(i,j-1).w_c\end{cases}}^{Type-1}..+min\overbrace{\begin{cases}\delta(i,j-1).w_a\\ \delta(i-1,j-2).w_b\\ \delta(i-1,j-1).w_c\\ \delta(i-2,j-1).w_d\\ \delta(i-1,j).w_e\end{cases}}^{Type-2} \tag{9}$$

where weighting coefficients are $\{w_a, w_b, w_c\} = \{1, 2, 1\}$ and $\{w_a, w_b, w_c, w_d, w_e\} = \{1, 3, 2, 3, 1\}$

4. Results and discussion

Four Nichrome-Heaters with adhered steel plates and thermocouples were used as thermal objects adjustable to three different temperatures, 30 °C, 300 °C and 425 °C. These temperatures may represent ‘‘Normal’’, ‘‘Critical’’ and ‘‘Over Critical‘‘ conditions. At ‘‘Critical’’ and ‘‘Over Critical‘‘ alarming actions can be taken. These thermal objects were placed at a distance of ten feet. Normalized response of the objects in four Fresnel zones at different temperatures are shown in Figs. 6a and b shows the simulated view of the objects.

In this study a Fresnel lens array modulated the four active zones with three level temperature scheme, indicated by 0, 1 and 2, thus there are 80 possible signatures can exist excluding [0000]. If digits 0, 1 and 2 represent 30 °C, 425 °C and 300 °C temperatures respectively, then with this ciphering e.g. a pattern [1102] indicates that zone-1 and zone-2 contains thermal objects at 425 °C, zone-3 at 30 °C and zone-4 at 300 °C. Fig. 6a shows 24 instances of four different temporal responses from a pool of 1920 signatures database. For selected patterns of [1110], [1210], [1120] and [1220], the figure also depicted large dissimilarities after sample count of 600, because up to this sample point only zone-1 stimulus generated that is identical for all these patterns.

In an experiment four thermal patterns [1110], [1210], [1220] and [1120] selected to elucidate the advantage of reduced length DTW and its preference over conventional DTW. Fig. 5 shows STFT reduced 3D DTW representation of these patterns indicating shortest warping gulley path, type-2 (and type-1) dynamic distances and local distances (D.Dist indicated on z-axis) between each point of reduced length time vectors. Table 1 summarizes type-1 and

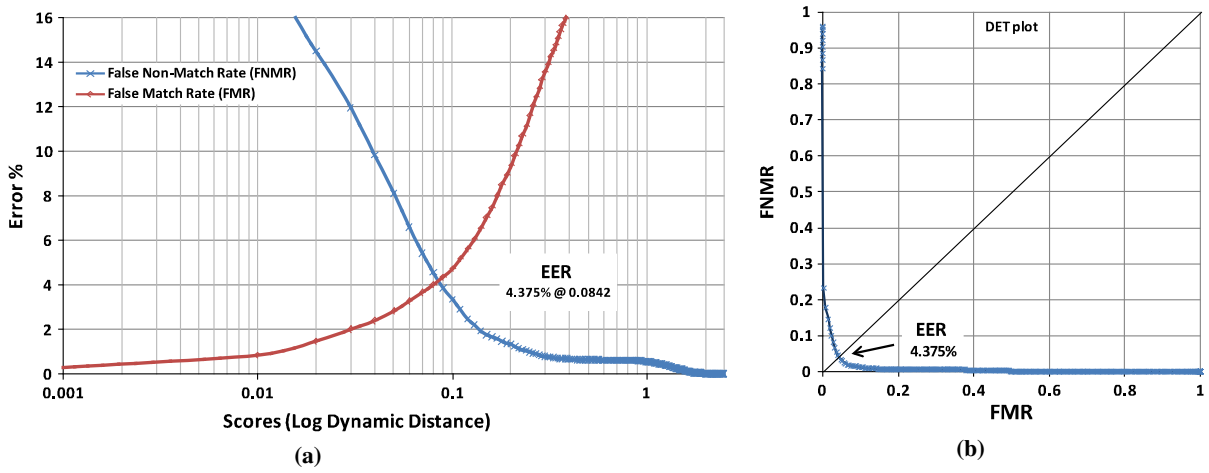

Fig. 11. (a) EER plot (b) DET plot.

type-2 shortest warping path scores and execution times for these patterns. In Fig. 5 warping path using type-2 DTW algorithm are shown by dark line starting at top corner and end at the bottom follow a route where the last point (i, j) on the dynamic path sees the shortest distance to the neighborhood points i.e.$(i, j\text{-}1)$, $(i\text{-}1, j\text{-}2)$, $(i\text{-}1, j\text{-}1)$, $(i\text{-}2, j\text{-}1)$, and $(i\text{-}1, j)$. From Table 1 it is evident that STFT reduced DTW is about 400 times faster than the DTW applied on full length vectors in both types, while scores farness, that is percent increase in scores of the same group to outside the group increases about 8% on average when DTW search criterion changes from type-1 to type-2. Further in type-2, scores are lower than in type-1 for the same group pattern matching, thus with STFT reduced type-2 DTW we can obtain quick identification with high true match and low false alarm rate.

Fig. 7 shows type-2 DTW log dynamic scores when all permuted sequences of thermal patterns [1 1 1 0], [1 2 2 0], [1 1 2 0] and [1 2 1 0] was excited and thermal gradient of the four active Fresnel zones identified within their respective groups with highest recognition rates. For [1 1 1 0] minimum scores found in its group of 24 samples range from 4×10^{-4} to 4×10^{-3}, it should be noted that the 2nd and 3rd closest match are [1 1 1 2] and [2 2 2 0] thermal patterns as expected. The reason behind is that the sensor sees the objects through 1st, 2nd, and 3rd Fresnel zones are at the highest temperature of 425 °C and dominantly control the shape of the response while the 2nd closest match [2 2 2 0] is due to the fact that it is a reduced gain version of [1 1 1 0]. Several other pattern sequences were generated and found the correct thermal gradient with average identification rate of 99.7% with the STFT abstracted type-2 DTW algorithm.

Fig. 8 shows thermal gradient field average identification results of two experiments for all permutations within the two selected pattern sets {|1 1 1 0|, |1 2 2 0|, |1 1 2 0|, |1 2 1 0|} and {|0 0 1 2|, |0 1 1 0|, |0 2 0 2|, |0 1 1 2|, |2 1 1 0|, |2 0 0 2|} of the registered objects with four Fresnel zones. Fig. 9 indicates the recognition rate increases with the larger database size of the training data sets, optimum 24 instances of each pattern produces estimable results. Fig. 10 shows average identification rates of each registered thermal pattern in 100 random sequences having all 80 thermal patterns. Each pattern database has first 24 STFT reduced vectors and utilizing type-2 DTW algorithm.

Table 2 provide false recognition match of testing patterns in column with the reference signals in row. All other 75 thermal patterns with database of 1800 samples have 0% false recognition with second minimum dynamic score. Detection-Error Tradeoff (DET) and Equal Error Rate (EER) plots of the abstracted DTW algorithm are shown in Fig. 11, which indicates EER of 4.3% when identical lowest DTW score of 0.0842 was chosen.

5. Conclusion

In this work we proposed a low cost, low power thermal field gradient detection scanner system based on a single node dual element pyroelectric infrared (PIR) sensor, a rotating aperture and a linear array of four Fresnel lenses that modulate the thermal radiation from four Fresnel zones. This scanner system can be used to monitor high tension nodes, or as a part of a surveillance system. The signal peaks, level degeneracy and polarity at an instant in the scanning phase correspond to the temperature variations in the Fresnel zones. A small temperature change, thermal gradient or movement of the object inside any Fresnel zone generate slightly different pattern that can be detected by measuring dynamic distances of the reduced STFT vectors with the registered patterns and identified in their clusters based on minimum DTW scores. In this work a three level temperature scheme and a linear array Fresnel lens was used that can be extended to multilevel.

Acknowledgments

The authors are grateful to the Dean Faculty of Science, University of Karachi for the financial grant, DFS-Grant/7960964/2011 for this research work and to Perkin Elmer Indonesia [14] for providing PIR sensors, also thankful to Mrs. Bilquees Rafique and Professor Dr. M. Ayub Khan Yousufzai for useful discussions.

References

[1] U. Gopinathan, D.J. Brady, N.P. Pitsianis, Coded Apertures for efficient pyroelectric motion tracking, Optics Express 11 (18) (2003) 2142.
[2] L. Peck, J. Lacombe, Environmentally dependent countermeasures to passive infrared detection, Army Cold Regions Research and Engineering Laboratory, US, 1998.
[3] P.J. Bauman, J.A. Jenks, D.E. Roddy, Evaluating techniques to monitor elk movement across fence lines, Wildlife Society Bulletin (1999) 344–352.
[4] H.A. Jacobson et al., Infrared-triggered cameras for censusing white-tailed deer, Wildlife Society Bulletin (1997) 547–556.
[5] D.L. Garshelis, P.L. Coy, B.D. Kontio, Applications of remote animal-activated cameras in bear research, International Union of Game Biologists (1994) 32–37.
[6] ELTEC Instruments, Inc. Parallel Opposed Dual IR Detector Model 442 IR-EYE integrated sensor.
[7] Sensor Technology Handbook by Jon. S. Wilson. Elsevier, ISBN: 0-7506-7729-5.
[8] Jian-Shuen Fang, Qi Hao, David J. Brady, Mohan Shankar, Bob D. Guenther, Nikos P. Pitsianis, Ken Y. Hsu, Path-dependent human identification using a

pyroelectric infrared sensor and Fresnel lens arrays, Jan 2006/Vol. 14, No. 2/ OPTICS EXPRESS.
[9] Mohan Shankar, John B. Burchett, Qi Hao, Bob D. Guenther, David J. Brady, Human-tracking systems using pyroelectric infrared detectors, Optical Engineering 45 (10) (2006) 106401-1. October.
[10] F. Xu, K. Fujimura, Pedestrian detection and tracking with night vision, in: Proceedings. IEEE Intelligent Vehicle Symp, 2002.
[11] 2. R. Bodor, B. Jackson, N. Papanikolopoulos, Vision-Based Human Tracking and Arecognition, in: Proceedings 11th Mediterranean Conference on Control and Automation, 2003.
[12] Fresnel Technologies Inc., <http://www.fresneltech.com>.
[13] Goran Dikic, Branko Kovacevic, Target Tracking with Passive IR Sensors, TELSIKS, NiS, Yugoslavia, 2001, pp. 19–21. September.
[14] Perkin Elmer optoelectronics. <www.perkinelmer.com/opto/lhi968>.
[15] Jacob Fraden, Handbook of Modern Sensor Physics, Design and Applications 3e, ISBN 0-387-00750-4, Springer-Verlag, Inc.
[16] H. Sakoe, S. Chiba, Dynamic programming algorithm optimization for spoken word recognition, IEEE Transactions Acoustics, Speech, and Signal Processings 26 (1978) 43–49.
[17] RSC-464 Speech Recognition and Synthesis Microcontrollers Application Document:80–0304-A. Copyright © 1994–2010 Sensory Inc.
[18] V.I. Levenshtein, Binary codes capable of correcting deletions, insertions, and reversals, Doklady Akademii Nauk SSSR (Russian) 163 (4) (1965) 845–848.
[19] Jian-Shuen Fang, Qi Hao, David J. Brady, Bob D. Guenther, Ken Y. Hsu. A pyroelectric infrared biometric system for real-time walker recognition by use of a maximum likelihood principal components estimation (MLPCE) method, 15(6) (2007) 19 March/Optics Express 3271.
[20] B. Ugur Toreyin, et al., Flame detection system based on wavelet analysis of pir sensor signals with an hmm decision mechanism, 16th European signal processing Conference (EUSIPCO 2008), Lausanne, Switzerland, 25th August 2008.